Controlling the Structure of Arenedisulfonates toward Catalytically Active Materials

Felipe Gándara,[†] Enrique Gutiérrez Puebla,[†] Marta Iglesias,[†] Davide M. Proserpio,[‡] Natalia Snejko,[†] and M. Ángeles Monge*,[†]

Instituto de Ciencia de Materiales de Madrid, CSIC, Madrid, Spain, and Dipartimento di Chimica Strutturale e Stereochimica Inorganica, Università di Milano, Milano, Italy

Received September 3, 2008

By adjusting the solvothermal synthesis conditions, two ytterbium catalytically active MOF (metal organic framework) materials aimed at two different heterogeneous processes have been obtained as pure phases. Yb-LRH belongs to the first family of layered rare-earth hydroxides (LRH). With a 2D structure, highly related to that of the layered doubles hydroxides, Yb-LRHs have cationic inorganic layers with formula $[Yb_4(OH)_{10}(H_2O)_4]_n^{2+}$ and is a very active and selective catalyst in the sulfide oxidation reaction. The second, Yb-RPF-5, is a 3D rare-earth polymeric framework material, with formula [Yb(OH)(2,6-AQDS)(H_2O)] (AQDS = anthraquinone-2,6-disulfonate). With lower coordination for the Yb atom and additional acidity from the coordinated ligands, it acts as a good catalyst in hydrodesulfurization (HDS) reactions. Both materials are bifunctional catalysts in redox and acid processes. Structural features of the materials, as well as their catalytic activity and topology, have been studied.

Introduction

The design and synthesis of new materials with desirable properties is one of the main purposes of solid-state chemistry. In this area, metal organic frameworks MOFs have received immense interest in the last years, because of their great possibilities in different applications,[1] such as heterogeneous catalysis.[2,3] On the other hand, layered double hydroxides (LDHs), also known as hydrotalcite-like materials or synthetic anionic clays, with a brucite-like structure and the formula $[M^{II}_{1-x}M^{III}_x(OH)_2]^{x+}(A^{n-})_{x/n}\cdot yH_2O$ have attracted increasing attention in recent years because of their potential applications as adsorbents, ionic conductors, and catalysts.[4]

In our ongoing research of rare-earth coordination networks,[5−7] we have reported in a recent communication[8] the first layered rare-earth hydroxide (LRH), a new type of layered[9] crystalline material very related with the LDH materials, in which the positive charge of the inorganic layer is created by varying the number of hydroxyl groups coordinated to the R^{3+} cation instead of introducing two different cations (as it occurs in LDH compounds). This arises from the high and variable coordinative capability of the rare-earth centers and to the tendency of the hydroxide ion to form μ_n connections in structures that contain these rare-earth centers. Rigid organic anions are intercalated to neutralize the positive charge.

One of the conclusions that could be deduced from the previous studies of LRH compounds is that to a certain extent, apart from the more convenient configuration of the organic linker, the LRH structure seemed to be kinetically favored for small rare-earth cations. However, previous screenings on the synthesis conditions did not rule out the possibility to obtain 3D materials also for the same linker and rare-earth cation. A correct choice of the synthesis conditions seems to be decisive to obtain either, 2D layered hydroxide or 3D polymeric framework material as pure phases. In this paper, we report the complete study of the different synthesis conditions that lead to the different structures, and thus to materials designed for heterogeneous catalysis of different specific reactions. A new rare earth polymeric framework (named Yb-RPF-5) compound has been obtained, and its structure, topology, and catalytic properties are here compared with those of the Yb-LRH

* To whom correspondence should be addressed. E-mail: amonge@icmm.csic.es.
† Instituto de Ciencia de Materiales de Madrid.
‡ Università di Milano.

(1) (a) Janiak, C. *Dalton Trans* **2003**, *14*, 2781. (b) James, S. L. *Chem. Soc. Rev.* **2003**, *32*, 276.
(2) (a) Alaerts, L.; Seguin, E.; Poelman, H.; Thibaul-Starzyk, F.; Jacobs, P. A.; De Vos, D. E. *Chem.—Eur. J.* **2006**, *12*, 7353. (b) Mueller, U.; Schubert, M.; Teich, F.; Puetter, H.; Schierle-Arndt, K.; Pastre, J. *J. Mater. Chem.* **2006**, *16*, 626. (c) De Rosa, S.; Giordano, G.; Granato, T.; Katovic, A.; Siciliano, A.; Tripicchio, F. *J. Agric. Food Chem.* **2005**, *53*, 8306. (d) Seo, J. S.; Whang, D.; Lee, H.; Jun, S. I.; Oh, J.; Jeon, Y. J.; Kim, K. *Nature* **2000**, *404*, 982. (e) Schlichte, K.; Kratzke, T.; Kaskel, S. *Microporous Mesoporous Mater.* **2004**, *73*, 81.
(3) Gándara, F.; Fortes-Revilla, C.; Snejko, N.; Gutiérrez-Puebla, E.; Iglesias, M.; Monge, M. A. *Inorg. Chem.* **2006**, *45*, 9680.
(4) Rives, V. *Layered Double Hydroxides: Present and Future*; Nova Science Publishers: New York, 2001.
(5) Snejko, N.; Cascales, C.; Gómez-Lor, B.; Gutiérrez-Puebla, E.; Iglesias, M.; Ruíz-Valero, C.; Monge, M. A. Chem. Comm. 2002, *1366*
(6) Gándara, F.; García-Cortés, A.; Cascales, C.; Gómez-Lor, B.; Gutiérrez-Puebla, E.; Iglesias, M.; Monge, M. A.; Snejko, N. *Inorg. Chem.* **2007**, *46*, 3475.
(7) Gándara, F.; de Andrés, A.; Gómez-Lor, B.; Gutiérrez-Puebla, E.; Iglesias, M.; Monge, M. A.; Proserpio, D. M.; Snejko, N. *Cryst. Growth Des.* **2008**, *8*, 378.
(8) Gándara, F.; Perles, J.; Snejko, N.; Iglesias, M.; Gómez-Lor, B.; Gutiérrez-Puebla, E.; Monge, M. A. *Angew. Chem., Int. Ed.* **2006**, *45*, 7998.
(9) (a) Holman, K. T.; Pivovar, A. M.; Swift, J. A.; Ward, M. D. *Acc. Chem. Res.* **2001**, *34*, 107. (b) Pivovar, A. M.; Holman, K. T.; Ward, M. D. *Chem. Mater.* **2001**, *13*, 3018. (c) Rusell, V. A.; Etter, M. C.; Ward, M. D. *J. Am. Chem. Soc.* **1994**, *116*, 1941.

10.1021/cm8029517 CCC: $40.75
Published on Web 01/22/2009

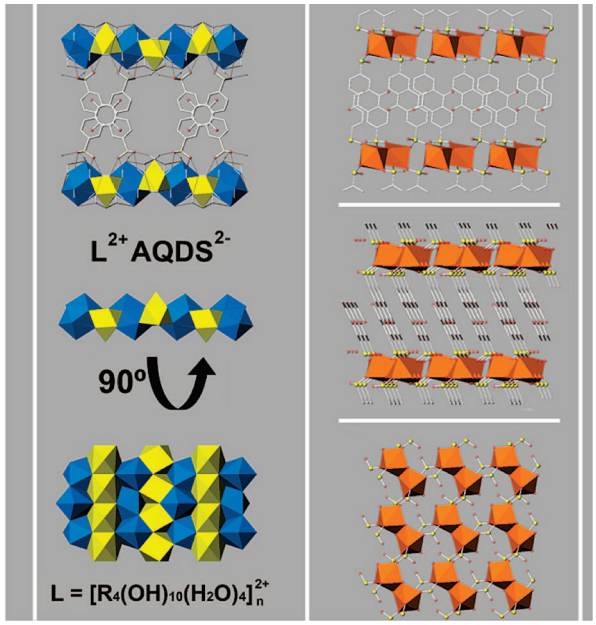

Figure 1. Left: Structure of Yb-LRH, $[Yb_4(OH)_{10}(H_2O)_4]$ [2,6-AQDS]. Right: Structure of Yb-RPF-5, $[Yb(OH)(2,6\text{-AQDS})(H_2O)]$.

material. In addition, a new refinement of the crystal structure for the Yb-LRH[8] is also included.

Experimental Section

General Information. All reagents and solvents employed were commercially available and used as supplied without further purification: anthraquinone-2,6-disulfonic acid disodium salt, 2,6-$AQDSNa_2$, (97% Sigma-Aldrich); ytterbium nitrate pentahydrate, $Yb(NO_3)_3 \cdot 5(H_2O)$, (99% Strem Chemicals). The IR spectra were recorded from KBr pellets in the range 4000−400 cm^{-1} on a Perkin-Elmer spectrometer. Thermogravimetric and differential thermal analyses (TGA-DTA) were performed using a SEIKO TG/DTA 320 apparatus in the temperature range between 25 and 800 °C in N_2 (flow of 50 mL/min) atmosphere and at a heating rate of 5 °C/min. A thermostar QMS200 M3 quadrupole mass spectrometer detector was employed. Power X-ray diffraction (PXRD) patterns were measured with a Bruker D8 diffractometer, with step size = 0.02° and exposure time = 0.5 s/step.

Synthesis. The compounds were synthesized under hydrothermal conditions, by heating an aqueous solution of molar compositions given in table 1, with a initial pH of 6.5, at 175 °C for 18 h in a Teflon-lined stainless steel autoclave. For Yb-LRH (ytterbium-layered rare-earth hydroxide), typically 0.112 g (0.25 mmol) of 2,6-$AQDSNa_2$ and 0.510 g (1 mmol) of $Yb(NO_3)_3 \cdot 5(H_2O)$ were dissolved in 19.8 mL of water (1100 mmol), and then 0.032 mL (2.375 mmol) of triethylamine was added. For Yb-RPF-5 (ytterbium-rare earth polymeric framework-5), 0.320 g (0.78 mmol) of 2,6-$AQDSNa_2$ and 0.350 g (0.78 mmol) of $Yb(NO_3)_3 \cdot 5(H_2O)$ were dissolved in 21.1 mL of water (1170 mmol), and then 0.77 mL of a 1 M solution of NaOH (0.77 mmol NaOH) was added. After being cooled to room temperature, the products were filtered and washed with deionized water and acetone. In all cases, the products were isolated as a unique phase: large yellow crystals of Yb-RPF compound (65% yield) and a grayish white powder of Yb-LRH compound (94% yield). Only a few single crystals of Yb-LRH were obtained. The purity of the products was tested by comparing the experimental and simulated PXRD patterns and through the elemental CHNS analysis. Calcd for Yb-LRH: C, 12.9; H, 1.8; S, 4.9. Found: C, 13.0; H, 2.2; S, 4.6. Calcd for Yb-RPF: C, 29.2; H, 1.6; S, 11.1. Found: C, 28.1; H, 1.7; S, 10.6.

Table 1. Synthesis Conditions

Yb/AQDS[a]	H_2O/AQDS[a]	base	product
4	4400	Et_3N	pure LRH phase
4	4400	Py	pure LRH phase
1	1500	NaOH	pure RPF phase
4	4400	NaOH	RPF majority phase + LRH presence
4	1500	NaOH	RPF + LRH
1	4400	Et_3N	pure LRH phase
1	1500	Et_3N	pure LRH phase

[a] Molar ratio.

X-ray Structure Determination. Single crystals suitable for X-ray crystallography were carefully selected and mounted in a Bruker SMART CCD diffractometer equipped with a normal focus, 2.4 kW sealed tube X-ray source (Mo Kα radiation = 0.71073 Å). Data were collected over a hemisphere of the reciprocal space by a combination of three sets of exposures. Each exposure of 20 s covered 0.3° in ϖ. Unit-cell dimensions were determined by a least-squares fit of 60 reflections with $I > 20\sigma(I)$. The structures were solved by direct methods. The final cycles of refinement were carried out by full-matrix least-squares analyses with anisotropic thermal parameters for all non-hydrogen atoms. Hydrogen atoms of the hydroxyl groups and water molecules were located in difference Fourier maps. Calculations were carried out with SMART software for data collection and data reduction and SHELXTL.[10]

Catalytic Experiments. Hydrodesulfurization of tiophene was carried out in a Parr reactor, under 7 bar of H_2. For tiophene decomposition, 10 mL (125 mmol) of substrate and 0.040 g of Yb-LRH or 0.072 g of Yb-RPF5 (0.125 mmol of Yb catalyst) were mixed and heated at different temperatures, with stirring. After selected time intervals, the reactor was cooled and then opened; the remaining amount of tiophene was then measured. For sulfide oxidation, 2 mmol of the substrate (methylphenylsulfide) was added to a flask containing a suspension of the Yb catalyst (0.002 mmol) in acetonitrile. Under stirring, and after being heated to 60 °C, an excess of the oxidant (5 mmol of H_2O_2) was added dropwise. For epoxidation of linalool, a suspension containing 1 mmol of the substrate and the catalyst (100:1 linalool:Yb) in 5 mL of acetonitrile was heated to 80 °C, under stirring. An excess of oxidant (H_2O_2) was then added. Chemical yield was measured by gas chromatography (GC), in a Hewlett-Packard 5890 II coupled with a mass detector. A methylsilicone column was employed.

Results and Discussion

Synthesis. As indicated in experimental section, time, pH, and temperature are similar for the synthesis of both compounds. From the synthesis conditions summarized in Table 1, some conclusions can be made: Despite the fact that for all the syntheses the pH is 6.5, the source of OH^- anions seems to be a decisive factor. When using an amine, the LRH phase is obtained, whereas with an inorganic base such as Na(OH), a mixture of 2D LRH and 3D RPF phases can appear independently of the reagent ratio (see the Supporting Information). The only way to get the 3D structure as single product is by adjusting its molecular formula with an equimolar amount of OH^- anions. It seems that the presence of any other different compound added to

(10) Software for the SMART System V5.04 and SHELXTL V 5.1; Bruker-Siemens Analytical X-ray Instrument Inc.: Madison, WI, 1998.

Table 2. Crystallographic Data for Yb-LRH and Yb-RPF-5

	Yb-LRH	RPF-5
empirical formula	$C_{14}H_{24}O_{22}S_2Yb_4$	$C_{14}H_9O_{10}S_2Yb$
fw	1300.61	574.37
cryst syst	orthorhombic	triclinic
space group	*Ibam*	$P\bar{1}$
a (Å)	12.5401(6)	7.3843(8)
b (Å)	35.6519(19)	7.8665(8)
c (Å)	7.0347(4)	13.7366(15)
α (deg)	90	86.119(2)
β (deg)	90	86.097(2)
γ (deg)	90	86.398(2)
Volume	3145.1(3)Å^3	792.90(15)Å^3
Z	4	2
Density(calculated)	2.747 Mg/m^3	2.406 Mg/m^3
Absorption coefficient	12.000 mm^{-1}	6.219 mm^{-1}
theta range for data collection (deg)	1.72−33.14	1.49−28.27
cryst size	0.20 × 0.10 × 0.05 mm^3	0.20 × 0.15 × 0.10 mm^3
independent reflns	2606 [*R*(int) = 0.0628]	3717 [*R*(int) = 0.0450]
data/restraint/params	2606/12/105	3717/1/244
GOF on F^2	1.024	1.036
final *R* indices [$I > 2\theta(I)$]	*R*1 = 0.0719, *wR*2 = 0.1883	*R*1 = 0.0560, *wR*2 = 0.1292
R indices (all data)	*R*1 = 0.0947, *wR*2 = 0.2007	*R*1 = 0.0678, *wR*2 = 0.1349

control the pH, such as triethylamine or pyridine in the mixture, releases more hydroxide anions as the reaction runs, in a such way that the formation of the cationic layer with a higher OH^-/Ln^{3+} ratio (molecular formula $[Yb_4(OH)_{10}]^{2+}$) is favored, and the Yb-LRH product is obtained. This factor seems to be more important than the possible amine template effect, or even the influence of the Bronsted/Lewis acid character of the used base.

Crystal Structure Description. Details of unit cell, data collection, and refinement for the two compounds are given in Table 2.

The molecular formulas of the two compounds are $[Yb_4(OH)_{10}(H_2O)_4]$ [2,6-AQDS] (Yb-LRH) and [Yb(OH)(2,6-AQDS)(H_2O)] (Yb-RPF-5) (2,6-AQDS = anthraquinone-2,6-disulfonate).

Yb-LRH. As we previously reported,[8] the structure of the LRH family of compounds is highly related to that of the LDH materials, with positively charged layers, and the anions situated in the interlayer space. The layers have a formula $[Yb_4(OH)_{10}(H_2O)_4]_n^{2-}$. Two crystallographically independent Yb atoms are found, with coordination numbers 8 and 9. Each Yb ion is coordinated to a water molecule and to the μ_3-hydroxyl groups, thanks to which the cations are linked giving rise to the inorganic layer. Two different coordination polyhedra are formed: one dodecahedron and a monocaped square antiprism. Polyhedra of the same type are placed in alternated rows parallel to the 001 direction forming the layers parallel to the ac plane. The $AQDS^{2-}$ anions are located in the interlayer space, linked to the layers through hydrogen bonds. They are highly ordered, with a titling angle formed between the organic anion S−S axes and the normal of the respective hydroxide layers of 30.86°. The value of the basal spacing is one-half of the *b* parameter. The $AQDS^{2-}$ anions are situated parallel to the ab plane in an alternated configuration, and separated 3.5 Å (*c*/2) and 12.5 Å (*a*) along the [001] and [100] directions, respectively (Figure 1, left).

This arrangement gives rise to $\pi-\pi$ and O−π stacking interactions of the parallel type[11] among the $AQDS^{2-}$ central rings and among one of the quinonic oxygen atoms and lateral aromatic rings, respectively, at a distance of 3.52 Å. Thanks to this well-ordered disposition of the anions in the interlayer space, this compound has a porous structure, with channels running along the *c* direction. The potential solvent area is 16.4%, as computed by Platon.[12]

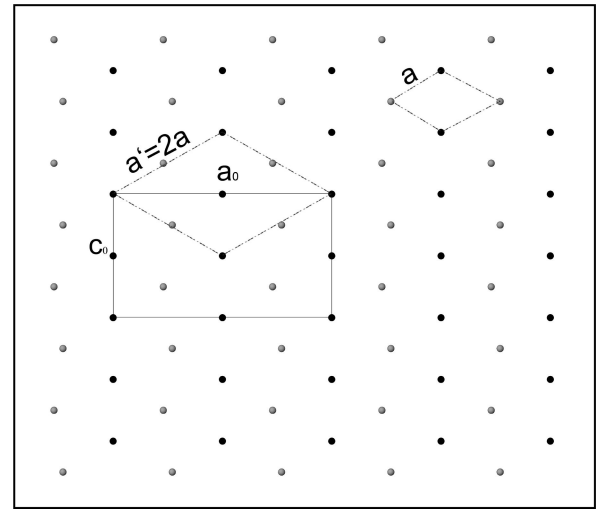

Figure 2. Crystallographic transformation from the LDH material structure to the new orthorhombic LRH structure.

From a crystallographic point of view, a direct relation exists between the brucite derived LDH hexagonal lattice and that of the LRHs. Given that in the latter there are two independent well-ordered Yb atoms by asymmetric unit, the ideal hexagonal superlattice would have an *a′* parameter twice that of the mineral. As the distances among Yb atoms are not uniform, this hexagonal superlattice is not real but it has a distortion that gives rise to orthorhombic larger cell for Yb-LRH compound. Vectors of the LRH unit cell can be deduced from those of the LDH by roughly applying the transformation matrix ($2\bar{2}0$, $00\bar{1}$, 220) (Figure 2).

In terms of topology, the cationic $[Yb_2(OH)_{10}]^{2+}{}_n$ layer can be described as a pentanodal 3,7,8 connected net, with stoichiometry $(3\text{-c})_5(7\text{-c})(8\text{-c})$, where the 7c and 8c nodes are given by the ytterbium atoms, and the 3c by the hydroxylic oxygen atoms (Figure 4, top left). To study the 3D net formed through the hydrogen bonds, the model has been simplified as follows: First of all, the oxygen atoms of the layer are omitted, giving rise to a (3,6) sheet of Yb atoms (Figure 3, top right). Second, the intercalated AQDS molecules are directly connected to the $[Yb_2(OH)_{10}]^{2+}$ layers via hydrogen bonds (Figure 3, bottom left). The result is a trinodal, octa- and pentaconnected net with stoichiometry $(5\text{-c})(8\text{-c})_2$, and point (Schläfli) symbol $(3^{10}.4^{12}.5^6)$ $(3^3.4^4.6^2.7^2)$ $(3^8.4^{11}.5^7.6^2)$ (Figure 3, bottom right).

Yb-RPF-5. The new **RPF-5** has a 3D structure, with the $AQDS^{2-}$ anions coordinated to the Yb atoms. Different from the Yb-LRH phase, in [Yb(OH)(2,6-AQDS)(H_2O)], the lanthanide ion is heptacoordinated (table 3,) to two μ_2-(OH) groups, one water molecule, and four oxygen atoms, belong-

(11) Janiak, C. *J. Chem. Soc., Dalton Trans.* **2000**, 3885.
(12) Spek, A. L. 2008 PLATON, A Multipurpose Crystallographic Tool; Utrecht University: Utrecht, The Netherlands.

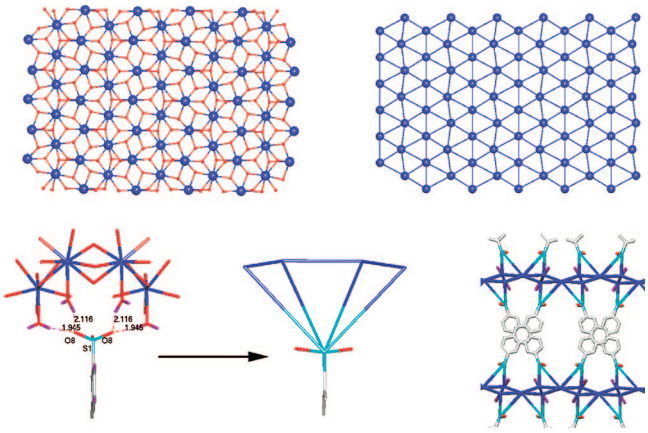

Figure 3. Topological analysis of Yb-LRH. Top, ball-and-stick (left) and simplified without oxygen atoms (right) view of the Yb−O layer; bottom, depiction of Yb-LRH structure considering hydrogen bonds.

ing to four different sulfonate groups in a YbO_7 monocaped trigonal prism. Every two of these (YbO_7) polyhedra form Yb_2O_{12} sharing edges dimeric units via two μ_2-OH^-, which are isolated in the *b* direction and joined through S atoms in the *a* direction. The SO_3 groups, with μ^2-η^2 coordination mode, join the $Yb_2(OH)_2$ units, with the S atom acting as a bridge between every two dimeric units in a such way that an entirely inorganic layer is formed parallel to the *ab* plane (Figure 1, bottom right). These layers are not as condensed as those of LRH, because they are 10R (6Yb + 4S) containing layers with the coordinated water molecules pointing inside the rings (in the LRH compounds, the coordinated water molecules point toward the interlamellar space and play a important structural role by forming the H-bonds with the intercalated AQDS molecules).

In the Yb-RPF-5 3D structure, the layers are connected along the *c* direction by $\eta^2\mu^2-\eta^2\mu^2$ bonded $AQDS^{2-}$ with a tilt angle of 66.27° between the *ab* plane, and that involving the three aromatic rings (Figure 1, right middle). These molecules are disposed along the 100 direction occupying two different position in the *b* axis, in an alternating configuration, and separated by 3.692 Å (*a*/2). Because the molecules in both position have the same slope trend, $\pi-\pi$ stacking interactions between rings are not given. In Figure 1, right top, the projection of the *bc* plane is shown.

From a topological point of view, we can describe an inorganic layer formed by the Yb atoms, where each atom is connected to the other three, one of them directly by hydroxyl groups and the other two through sulfonate bridges, resulting in a (6,3) honeycomb layer (Figure 4, left). The three-dimensional real net, with these layers linked through the whole ligand, can be described as a binodal net, where the S atoms are 3-connected nodes, and the ytterbium atoms are 5-connected nodes (Figure 4, middle). This network, with poing (Schläfli) symbol $(4.6^2)_2(4^2.6^2.8^6)$ has maximum symmetry in the space group *Fmmm* and it is found with the code sqc707 in the EPINET database,[13] where no previous examples of networks with this topology are described (Figure 4, right). Topological study of both Yb-LRH and Yb-RPF-5 structure was made with TOPOS.[14]

The comparison of the experimental and simulated X-ray powder diffraction patterns shows that both compounds appear as the only product of their respective optimized reactions. The X-ray patterns also demonstrate a high crystallinity of the obtained materials. Figure 5 shows both experimental and simulated patterns.

Thermal Behavior. *Yb-LRH.* TGA-DTA analysis (Figure 6) shows a first mass loss (3.5%) before 60 °C, which is due to the loss of adsorbed water molecules. In the temperature range of 100−400 °C, there are three steps in the TG curve, corresponding to a total mass loss of ∼10%. Only the signal corresponding to a mass of 18 was found in the mass detector in this temperature range. Consequently, a loss of 7 water molecules is assumed from the TG value (calculated value = 9.7%). Four of them are the 4 coordinated water molecules, present in the initial structure. The remaining three molecules come from the inorganic layer, in such a way that the formula of this layer after the heating, should be $[Yb_4O_3(OH)_4]^{2+}$. An elemental analysis made to the sample after being heated at 500 °C (under the same conditions than in the TG experiments) shows that all the organic components remain in the structure. The result of this analysis (14% C, 0.6% H, and 5.1% S) demonstrates that the $AQDS^{2-}$ anion remains intact in the structure (experimental C/S = 7.3, calculated = 7.0). The PXRD patterns of the heated samples show no changes in the peaks positions until 300 °C (Figure 7). At this temperature, a shift in the first peak to higher angle happens, and consequently, a diminution of the basal space to a value of 17.0 Å. Only the three first peaks are observed, indicating that the layered structure remains, but the layer is not so ordered. Finally, at 500 °C, a new diminution of the interlayer space takes place, with a final basal space of 16.5 Å, before the decomposition of the structure begins.

RPF-5. The first mass loss starts at ∼285 °C, corresponding to the loss of the only water molecule present in the structure (experimental 3%, calculated 3.1%). There is an irreversible phase transition associated to this change, showing the PXRD pattern a different crystalline phase when the sample is heated above this temperature (see the Supporting Information). This crystalline phase remains until the decomposition of the product, which begins at ∼485 °C. After an initial weight lost of ∼21% in a 80 degrees interval, the product decomposes gradually until a final weight loss of ∼62%, which indicates the almost total loss of the organic molecule (calculated = 69.6%). PXRD shows ytterbium oxide as main final residue, and the difference in percent mass loss is probably due to the presence of coke residue.

FTIR. The band (3300−3650 cm^{-1}) corresponding to the ν(Yb-OH) frequencies of the coordinated hydroxyl groups and water molecules is more narrow in the IR spectra of **Yb-RPF-5** compound than in the **Yb-LRH**, which has a broadband at 3000−3700 cm^{-1}. This broadening is due to the hydrogen bonds between the coordinated oxygen atoms

(13) Hyde, S.; Friedrichs, O. D.; Ramsden, S. J.; Robins, V. *Solid State Sci.* **2006**, *8* (7), 740.

(14) (a) BlatovV. A. *IUCr Compcomm Newsletter* **2006**, *7*, 4; http://www.topos.ssu.samara.ru. (b) Blatov, V. A.; Carlucci, L.; Ciani, G.; Proserpio, D. M. *CrystEngComm* **2004**, *6*, 377.

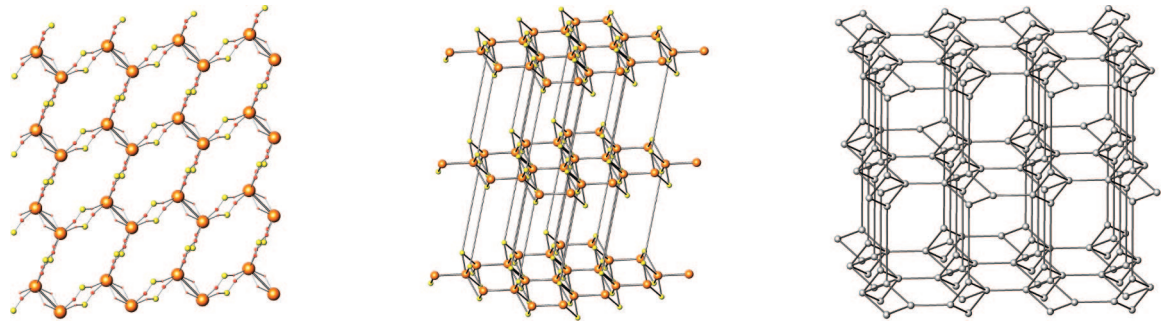

Figure 4. Topological analysis for Yb-RPF-5 showing: left, honeycomb inorganic layer; middle, simplified 3D real net; right, idealized $(4.6^2)_2(4.^26.^28^6)$ network.

Table 3. Bond Lengths (Å) in Yb-LRH and Yb-RPF-5

		LRH[a]	
O(1)−Yb(1)	2.538(11)	O(3)−Yb(2)	2.430(8)
O(2)−Yb(1)	2.275(12)	Yb(2)−O(3)#8	
O(3)−Yb(1)#3	2.242(8)	O(4)−Yb(2)#5	2.415(7)
Yb(1)−O(3)#2		O(4)−Yb(2)	
Yb(1)−O(3)#3		Yb(2)−O(4)#8	
O(5)−Yb(1)	2.386(15)	O(6)−Yb(2)	2.79(2)
O(4)−Yb(1)#3	2.274(11)	Yb(1)−Yb(2)#2	3.5221(6)
Yb(1)−O(4)#3		Yb(1)−Yb(2)#3	
Yb(1)−O(3)#4	2.324(8)	Yb(2)−Yb(1)#3	
O(3)−Yb(1)		Yb(1)−Yb(1)#6	3.7362(5)
O(1)−Yb(2)#2	2.300(7)	Yb(1)−Yb(1)#3	3.5173(2)
O(1)−Yb(2)#3		Yb(2)−Yb(2)#4	
Yb(2)−O(1)#7		Yb(2)−Yb(2)#5	
Yb(2)−O(1)#3			
O(2)−Yb(2)	2.392(7)		
O(2)−Yb(2)#4			
Yb(2)−O(2)#8			
		PPF[b]	
Yb(1)−O(9)	2.183(6)	Yb(1)−O(3)	2.299(6)
Yb(1)−O(9)#1	2.199(6)	Yb(1)−O(5)	2.310(6)
Yb(1)−O(6)	2.282(6)	Yb(1)−O(10)	2.325(7)
Yb(1)−O(2)	2.283(6)	Yb(1)−Yb(1)#1	3.5954(7)

[a] Symmetry transformations used to generate equivalent atoms: #1 $-x, -y + 1, -z + 1$ #2 $-x + 1/2, -y + 1/2, z + 1/2$ #3 $-x + 1/2, -y + 1/2, -z + 1/2$ #4 $x, y, -z + 1$ #5 $x, y, -z$ #6 $-x + 1/2, -y + 1/2, -z + 3/2$ #7 $x - 1/2, -y + 1/2$, z #8 $-x + 0, y + 0, -z + 1/2$. [b] Symmetry transformations used to generate equivalent atoms: #1 $-x, -y + 2, -z + 1$.

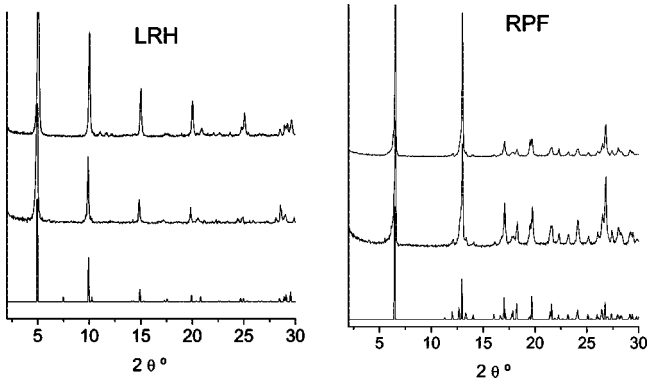

Figure 5. Comparison of the calculated (lower) and experimental powder X-ray diffraction pattern before (medium) and after (upper) catalytic reactions.

and the sulfonate group. In **Yb-RPF-5**, the coordination of the SO_3 group to the metal causes a shift of the band at 1040 cm^{-1} to higher wavenumber (∼1060 cm^{-1}), while in **Yb-LRH**, the uncoordinated $-SO_3$ group gives rise to nonsplitted bands in the region 1000−1100 cm^{-1}, corresponding to the C_{3v} symmetry that the group retains.

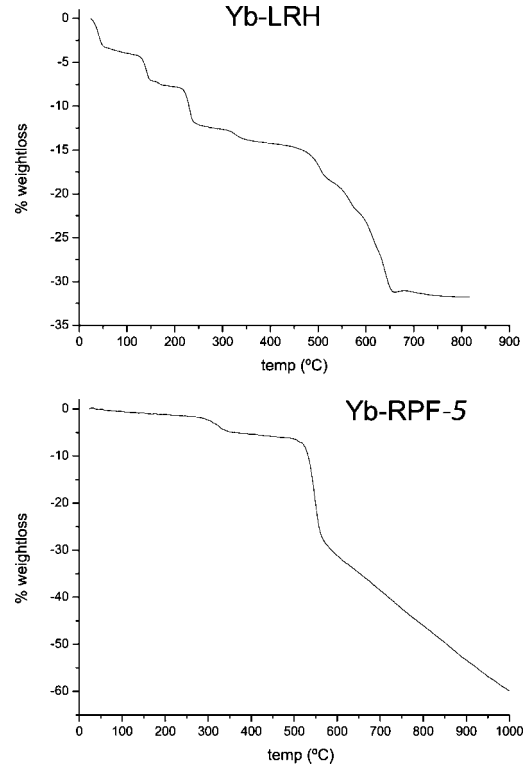

Figure 6. TG curves for Yb-LRH and Yb-RPF5.

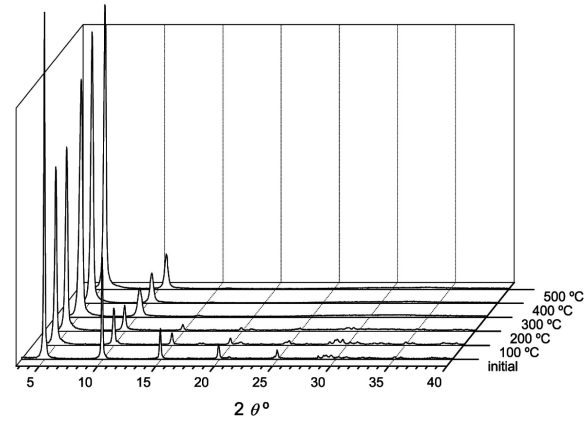

Figure 7. PXRD patterns of Yb-LRH heated samples.

Catalytic Activity. Rare earth metals are increasingly used as catalysts in a wide variety of organic transformations. MOF materials of these elements offer the possibility of combining the Lanthanide catalytic properties with the advantages of being heterogeneous catalysts. Both Yb-LRH

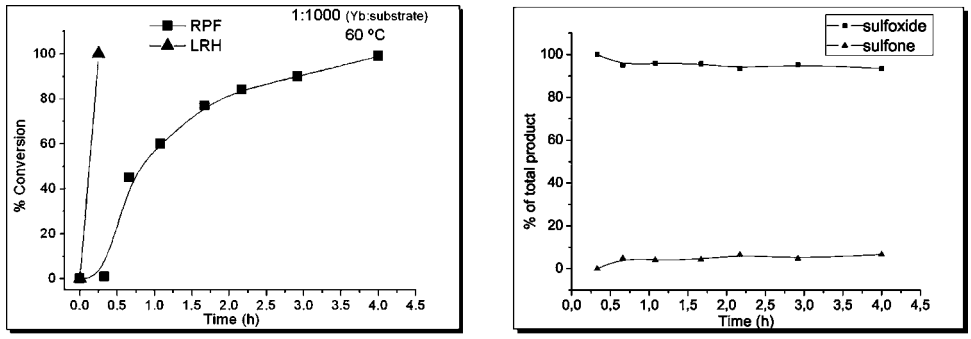

Figure 8. (Left) Kinetic profile and (right) selectivity curves of the oxidation of sulfides for Yb-RPF-5.

and Yb-RPF-5 materials bear a great number of active centers with capability of varying the coordination number in catalytic processes, which confers them great possibilities in the green chemistry field. These compounds help to control the activity and selectivity of a catalytic process by tuning geometrical features of their frameworks. The differences in the coordination environment of the active rare earth metal will lead to materials with specific activities in different catalytic processes. The properties of the new materials as heterogeneous catalysts have been tested in key processes, such as:

Hydrodesulfurization of Thiophene (HDS). The Yb-LRH under 7 bar of H_2 at only 70 °C shows a conversion of 50% in 26 h, with a ratio substrate/Yb = 1000, giving hydrogen sulfide and butane (both components easily separable). It is worth pointing out that these results are obtained under much milder conditions than those usually utilized (high pressure of H_2, i.e., 30−60 bar, at 350−400 °C[15,16]). For the Yb-RPF-5, a higher grade of conversion is obtained with the same rate of substrate vs active center and the total decomposition of the thiophene is achieved after 24 h. By increasing the temperature, the reaction becomes faster in such a way that only 16 h are needed at 100 °C, and a conversion of 90% is found after only 4.3 h at 120 °C. Although the Yb-RPF-5 structure is less open than that of Yb-LRH and thus, the catalytic reaction should take place only on surface, the activity of the former is higher because of the low Yb coordination number in this compound, which allows an easier access of the substrate to the active center, and to the acidity coming from the coordinated ligand, that favors the heterolytic rupture of the hydrogen molecule.

Oxidation of Sulfides. As an alternative to hydrodesulfurization reactions the removal of refractory sulfur containing compounds can be accomplished by oxidation. The present systems also catalyze the oxidation of various alkyl phenyl sulfides (figure 8).

Yb-LRH. Sulfides were selectively mono-oxygenated to the corresponding sulfoxides (100%) in 30 min, using H_2O_2 as oxidant. It is remarkable the excellent TOF = 2000 h^{-1} value reached by the material, due to the small quantity of catalyst (0.1%) needed and the fast conversion of the substrate[17] (TOF = turnover frequency, here defined as [mol substrate]/[mol Yb h]). Its activity is comparable to that of microporous bifunctional titanium aluminosilicates, and better, both in activity and selectivity, than that of previously studied rare earth succinate polymeric framework.[18]

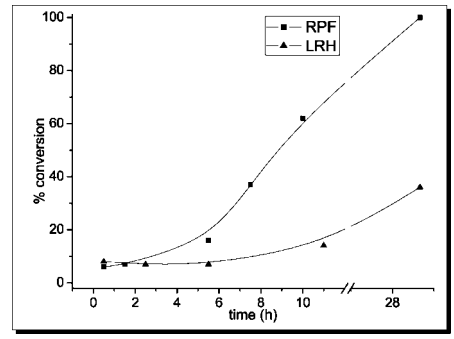

Figure 9. Catalytic activity of both materials for the conversion of linalool.

Yb-RPF-5 also presents catalytic activity, with a TOF value of 706 h^{-1} at 60 °C, which is smaller than that of Yb-LRH compound. The catalyst is highly selective, with the sulfoxide (>90%) being the main product of the oxidation. Kinetic profile and selectivity curve of the oxidation of sulfides are shown in Figure 8 left and right, respectively.

From a reaction mechanism viewpoint, the sulfooxidation reaction has to go through the corresponding peroxo species, as happens in the hydrolysis of phosphodiesters[19] and RNA,[20] catalyzed by peroxide rare earth complexes formed in rare earth−H_2O_2 mixtures. Accordingly, the different catalytic behavior of the two compounds in sulfides oxidation is a consequence of the different charge density over the rare earth cation, caused by the ligand nature: In the cationic layer of **Yb-LRH**, the coordination sphere of the Yb atom is composed only by oxygen atoms of μ_3-OH anions and one water molecule. In the 3D Yb-RPF-5, the charge density over the Yb cation is higher, because most oxygen atoms of the coordination sphere come from SO^{3-} groups, and thus, the formation of the active peroxo complex is slower when using this later system as catalyst.

Oxidation of Linalool. The two materials were also tested as bifunctional redox-acid catalyst in the transformation of 3,7-dimethylocta-1,6-dien-3-ol (linalool) to hydroxy ethers

(15) Sharma, K. R.; Olson, E. S. *Catalytic Hydrodesulfurization with Hydrotalcites, Processing and Utilization of High-Sulfur Coals IV*. Elselvier Science Publisher B.V.: Amsterdam, 1991; p 377.
(16) Chapus, T.; Morel, F. U.S. Patent 2002195375.
(17) Corma, A.; Iglesias, M.; Sánchez, F. *Catal. Lett.* **1996**, *39*, 153.
(18) Perles, J.; Iglesias, M.; Ruiz-Valero, C.; Snejko, N. *J. Mater. Chem.* **2004**, *14*, 2683.
(19) Mejia-Radillo, Y.; Yatsimirsky, A. *Inorg. Chim. Acta* **2002**, *328*, 241.
(20) Kamitani, J.; Sumaoka, J.; Asanuma, H.; Komiyama, M. *J. Chem. Soc., Perkin Trans.* **1998**, *2*, 523.

Scheme 1. Transformation of Linalool Reaction

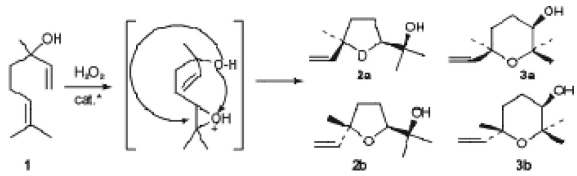

(furanoid and pyranoid forms, 2 and 3 in Scheme 1), in acetonitrile, at 353 K, with an excess of H_2O_2. In the reaction scheme, the first step involves the epoxidation of the 2,3 double bond, promoted by the metal as active center. In the second step, the presence of acid sites is needed for the intramolecular opening of the epoxide ring by the hydroxyl group at position 6 or 7. As it has been shown above, the Yb-LRH material is very active as redox catalyst but acts poorly as acid catalyst, so that only 36% of conversion occurs after 28 h, with a ratio 1:100 Yb:substrate. In the case of Yb-RPF-5, a total conversion is achieved after 28 h, with the same Yb:substrate ratio, and with a high selectivity to the furanoid versus pyranoid products (9:1 in the first run; 7:3 in the second run). Figure 9 shows the activity of both products for the oxidation of linalool.

Recycling Experiments. To verify the observed catalysis is truly heterogeneous, the catalytic reactions were carried out under standard conditions. After ~30% conversion, the solid was removed by filtration. The reactions were completely stopped when removing it. The solid was then used again without any loss of catalytic performance. X-ray diffraction powder pattern of the recovered catalysts showed no change in their structures. The analysis of ytterbium content (measured by ICP emission spectroscopy) in the solution after removal of the active Yb catalyst shows that only a 1% of the solid has been dissolved during the catalytic experiment. The PXRD patterns of the solids after the experiments show that no changes have occurred in the structure (Figure 3).

Conclusions

In summary, by controlling the source of hydroxyl anions in a mild hydrothermal method of synthesis and starting from the same components, that is, ytterbium and anthraquinone-2,6-disulfonate, two active catalytic materials aimed at two different heterogeneous processes have been obtained as pure phases. $[Yb_4(OH)_{10}(H_2O)_4]$ [2,6-AQDS] (Yb-LRH) has a 2D structure with cationic inorganic layers that make this material a very active and selective catalyst in sulfides oxidation.

[Yb(OH)(2,6-AQDS)(H_2O)] (Yb-RPF-5) with a 3D structure, in which the Yb cation bears more charge density, yields in poorer activity in sulfides oxidation reaction. However, the Yb low coordination number and the additional acidity coming from the coordinated sulfonate ligands make this material a good catalyst in hydrodesulfurization of thiophene (HDS) reactions.

Both materials behave as bifunctional catalyst for catalyzed redox and acid processes.

Acknowledgment. F.G. acknowledges a FPI fellowship from Ministerio de Educación y Ciencia (MEC) and Fondo Social Europeo from the EU. This work has been supported by the Spanish MCYT Project Mat 2007-60822, CTQ MAT 2006-14274-C02-02, and Consolider-Ingenio CSD2006-2001.

Supporting Information Available: X-ray crystallographic files in CIF format; PXRD patterns (PDF). This material is available free of charge via the Internet at http://pubs.acs.org.

CM8029517